ICHEP'98 #125
Submitted to Pa 1, 8
Pl 1

DELPHI 98-103 CONF 171
22 June, 1998

Measurement of $A_{FB}^{b\bar{b}}$ in Hadronic Z Decays using a Jet Charge Technique

Preliminary

DELPHI Collaboration

B. Überschär [1], **M. Elsing** [2], **U. Flagmeyer** [1], **K. Hamacher** [1], **K. Mönig** [3], **K. Münich** [1], **A. Passeri** [4]

Abstract

The $b\bar{b}$ forward-backward asymmetry ,$A_{FB}^{b\bar{b}}$, is determined from the average charge flow, $\langle Q_{FB} \rangle$, measured in a sample of 3 500 000 hadronic Z decays collected with the DELPHI detector in 1992 - 1995. The measurement is performed in an enriched $b\bar{b}$ sample selected using an impact parameter tag and results in :

$$A_{FB}^{b\bar{b}} \quad = \quad 0.0979 \pm 0.0047(\text{stat.}) \pm 0.0021(\text{syst.})$$

The $b\bar{b}$ charge separation, δ_b, required for this analysis is directly measured in the b tagged sample, while the other charge separations, $\delta_{d,u,s,c}$, are obtained from a fragmentation model precisely calibrated to data.
The effective weak mixing angle, $\sin^2\theta_{\text{eff}}^{l}$, is deduced from the measurement:

$$\sin^2\theta_{\text{eff}}^{l} \quad = \quad 0.2320 \pm 0.0009$$

Paper submitted to the ICHEP'98 Conference
Vancouver, July 22-29

[1] Fachbereich Physik, BU-GH Wuppertal, Gaußstraße 20, 42097 Wuppertal, Germany
[2] CERN, European Organisation for Particle Physics, CH-1211 Geneva 23, Switzerland
[3] DESY-Zeuthen, Platanenallee 6, 15738 Zeuthen
[4] INFN, Istituto Superiore di Santià, Viale Regina Elena 299, IT-00161 Rome, Italy

1 Introduction

The coupling of the Z boson to the fermions results in an asymmetric angular distribution of the $e^+e^- \to Z \to f\bar{f}$ final states. In terms of the vector and axial vector couplings (v_f, a_f), at $\sqrt{s} = M_Z$ the Standard Model predicts for the forward-backward asymmetry of the $f\bar{f}$ final state to the lowest order :

$$A_{FB}^{f\bar{f}} = \frac{3}{4} \frac{2a_e v_e}{a_e^2 + v_e^2} \frac{2a_f v_f}{a_f^2 + v_f^2} \tag{1}$$

Higher order electroweak corrections can be accounted for by means of an improved Born approximation, which leaves the above relation unchanged but defines the modified couplings $\bar{a}_f$, $\bar{v}_f$, and an effective mixing angle $\theta_{\rm eff}^l$ for which

$$\frac{\bar{v}_f}{\bar{a}_f} = 1 - 4|q_f| \sin^2 \theta_{\rm eff}^l \tag{2}$$

where q_f is the fermion electric charge. Therefore $\sin^2\theta_{\rm eff}^l$ includes higher order effects, and its measurement is an important test of the Standard Model predictions.

It is advantageous to measure asymmetries for quark final states as here in principle the sensitivity to $\sin^2\theta_{\rm eff}^l$ is larger compared to lepton final states. These measurements determine $\sin^2\theta_{\rm eff}^l$ as defined by the electron couplings [1].

Information on the original quark charges for these events has to be obtained from the final state hadrons. In this paper a momentum weighted average of the particle charges detected in one hemisphere (or clustered in one jet) was used. The difference Q_{FB} (often called *charge flow*) between the forward and backward hemisphere charges in each event, turns out to be a linear combination of the quark asymmetries, with coefficients mainly given by the charge separations δ_f, i.e. the quark-antiquark separation power of the hemisphere charge for each individual flavour. Any measurement of $\langle Q_{FB} \rangle$ and of the δ_f's then implies a measurement of $\sin^2\theta_{\rm eff}^l$. Flavour tagging techniques can give access to single flavour asymmetries.

In this paper the measurement of $\langle Q_{FB} \rangle$ is presented using a $b\bar{b}$ enriched sample. The $b\bar{b}$ forward-backward asymmetry ,$A_{FB}^{b\bar{b}}$, has been determined from this measurement and the effective weak mixing angle, $\sin^2\theta_{\rm eff}^l$, was derived.

In this section a short discussion of the principles underlaying the jet charge technique and the the basic definitions which will be used throughout the paper are given. The DELPHI detector and the event selection are described in section 2, together with the b tagging technique used to obtain $b\bar{b}$ enriched samples. In section 3 the determinations of the individual charge separations are described: δ_b was directly measured from the data, while the other charge separations $\delta_{d,u,s,c}$ were obtained from an accurately tuned fragmentation model. In section 4 the $A_{FB}^{b\bar{b}}$ extraction is described, and the systematic errors are discussed in section 5. Finally a summary and conclusion are presented in section 6.

In order to measure charge asymmetries in the process $e^+e^- \to Z \to q\bar{q} \to$ jets it is necessary to determine the charge of the quarks underlying hadron jets in an event. The quark charge has to be determined from the final state hadrons and therefore this information is smeared by the fragmentation process.

Experimentally the charge of the initial fermion in the related hemisphere is estimated using the following hemisphere charge definition:

$$Q_{F(B)} = \frac{\sum_i q_i |\vec{p_i} \cdot \vec{T}|^\kappa}{\sum_i |\vec{p_i} \cdot \vec{T}|^\kappa} \qquad \begin{array}{ll} F : \vec{p_i} \cdot \vec{T} > 0 & \text{forward hemisphere} \\ B : \vec{p_i} \cdot \vec{T} < 0 & \text{backward hemisphere} \end{array} \tag{3}$$

where the sum runs over the charged tracks, $\vec{T}$ is the Thrust unit vector, q_i the particle charge, $\vec{p_i}$ the particle momentum and the exponent κ a positive number. The plane perpendicular to the Thrust axis computed using charged and neutral particles divides each event into two hemispheres. The Thrust axis orientation was always chosen to point into the same direction as the incoming electrons.

Consistency of the results over a wide range of κ choices ($\kappa = 0.3, 0.5, 0.8, 1, 1.2, 2.1$) is used to justify the obtained precision of the results. This observable is robust against mismeasurement of the hadron momenta $\vec{p_i}$. Its value is bound in the interval -1 to 1. The projection of the hadron momenta to the Thrust axis $\vec{T}$ projects out the influence of hard gluon radiation.

For every event two quantities the charge flow, Q_{FB}, and total charge, Q_{TOT}, can be defined :

$$Q_{FB} = Q_F - Q_B \tag{4}$$

$$Q_{TOT} = Q_F + Q_B \tag{5}$$

Except for detector influences (mainly hadronic re-interaction) the averaged total charge $\langle Q_{TOT} \rangle$ is expected to vanish, while the average charge flow $\langle Q_{FB} \rangle$ relates to the relevant quark asymmetries:

$$\langle Q_{FB} \rangle = \sum_{flavours\ \mathrm{f}} \eta_\mathrm{f} \delta_\mathrm{f} P_\mathrm{f} A_{FB}^{\mathrm{f\bar{f}}}. \tag{6}$$

η_f is a weighting factor to account mainly for the incomplete angular acceptance, limited angular resolution and other detector effects, but also for the QCD correction. P_f is the relative abundance of a quark flavour f in the hadronic event sample.

The overall impact of fragmentation in $\mathrm{e^+e^-}$ annihilation events into a given quark flavour f can be judged from the average difference of the hemisphere charge in the hemisphere of the quark f and the anti-quark $\bar{\mathrm{f}}$:

$$\delta_f(\kappa) = \langle Q_f - Q_{\bar{f}} \rangle(\kappa) \tag{7}$$

This quantity is called charge separation, δ_f, and if quarks could be directly observed $\delta_\mathrm{f} = 2q_\mathrm{f}$. In case of a pure flavour sample, which is approximately the case for the b tagged sample, δ_f can be measured from the data using the relation:

$$\delta_\mathrm{f}^2 = (\sigma_{FB}^\mathrm{f})^2 - (\sigma_{TOT}^\mathrm{f})^2 \tag{8}$$

Here $(\sigma_{FB}^\mathrm{f})^2$ and $(\sigma_{TOT}^\mathrm{f})^2$ is the variance of the Q_{FB} , respectively Q_{TOT}, distribution. The validity of this equation is immediately evident from Fig.1. Note, however, that charge correlations between the event hemispheres are neglected in this expression.

To measure $A_{FB}^{\mathrm{b\bar{b}}}$ Eqn.6 was used, and all quantities appearing in it were evaluated. $\langle Q_{FB} \rangle$ was directly measured from the data as well as P_b and δ_b with a minimal input from simulation; $P_{\mathrm{f}\neq\mathrm{b}}$, $\delta_{\mathrm{f}\neq\mathrm{b}}$ and η_f were determined using simulated events. The relation between $A_{FB}^{\mathrm{b\bar{b}}}$ and $A_{FB}^{\mathrm{c\bar{c}}}$ was taken from the SM prediction and up type (down type) quark universality has been assumed.

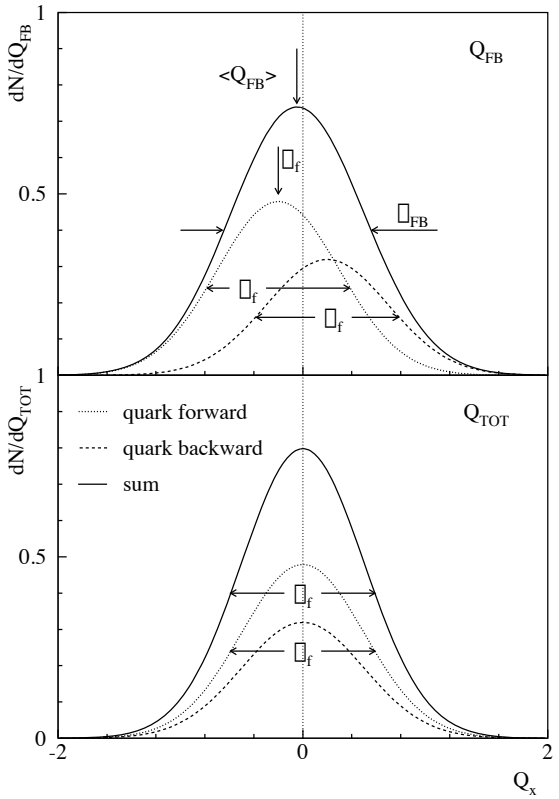

Figure 1: Sketch of the principle of the $\langle Q_{FB} \rangle$ and the δ_{f}^2 measurement for a single (down type) flavour f. σ_{f} is the RMS of the Q_{TOT} ($\rightarrow \sigma_{TOT}^{\mathrm{f}}$) distribution or of the Q_{FB} distribution for quarks going only to the forward (backward) direction, respectively. σ_{FB} is the RMS of the overall Q_{FB} ($\rightarrow \sigma_{FB}^{\mathrm{f}}$) distribution.

2 Detector description and event selection

2.1 The DELPHI detector

The DELPHI detector has been described in details in [2].

In the DELPHI coordinate system the z-axis is parallel to the beam pointing into the flight direction of the electrons. The radius R and the azimuth ϕ are defined in the plane perpendicular to z and the polar angle θ is 0 along z. Only the detector components which were used in this analysis are mentioned here.

In the barrel part a set of cylindrical detectors, coaxial with the beam direction and inside a 1.2 T solenoidal magnetic field, are devoted to the measurement of the charged particle tracks. The innermost is the Vertex Detector (VD) [3], located just outside the beam pipe. It consists of three concentric layers of silicon micro strip detectors at average radii of 6.3 cm, 8.8 cm and 10.9 cm from the interaction region and it covers a polar angle range between 27° and 153°. Until 1993 it provided only measurements of the $R\phi$ coordinate. In 1994 the innermost and the outermost VD layers were equipped with double sided silicon detectors, which allowed to measure also the z coordinate.

Outside the VD, between 12 cm and 28 cm of radius, there is the Inner Detector (ID), which is composed by a jet chamber providing up to 24 $R\phi$ measurements and by five layers of proportional chambers providing both $R\phi$ and z information. The ID covers the θ range between 29° and 151°. It is surrounded by the Time Projection Chamber (TPC), the main DELPHI tracking device, which is a cylinder of 3 m length, an inner radius of 30 cm and an outer radius of 122 cm. The ionization charge produced by particles crossing the TPC volume is drifted to the edges of the detector where it is measured in a proportional chamber. Up to 16 space points can be measured, for $39° < \theta < 141°$. Outside this region, and up to 21° and to 159°, a track can be reconstructed using at least 3 points. Additional $R\phi$ measurements on the charged particles tracks are provided by the Outer Detector (OD), which lays between radii of 198 cm and 206 cm and consists of five layers of drift cells. In the forward region two sets of wire chambers (FCA, FCB), at $\pm$160 cm and at $\pm$270 cm in z, provided measurements of low angle particles trajectories.

The electromagnetic calorimeters HPC in the barrel and FEMC in the forward region were used to measure electromagnetic interacting particles.

2.2 The sample of hadronic events

The track cuts are optimised to ensure well measured tracks for the analysis. The event cuts are chosen to reduce the background arising from lepton and $\gamma\gamma$ events as well as from beam-gas or beam-wall events. After the selection the contribution of background events turns out to be negligible. To ensure a good measurement of the forward and backward hemisphere charges hemisphere related cuts were applied.

Events containing one or more tracks with momentum greater than 50 GeV were discarded.

The angular acceptance is limited by detector effects entering into the measurement of the hemisphere charge :

- the angle between momentum vector and magnetic field affects the detector resolution.

track cuts	$\mid \vec{p} \mid$	$\geq$	$0.4\,GeV/c$
	e_{neu}	$\geq$	$0.5\,GeV$
	$t_{len}^{\text{TPC only}}$	$\geq$	$30\,cm$
	$\theta_{ch(neu)}$	$\geq$	$20^\circ(11^\circ)$
	$\frac{\Delta\mid\vec{p}\mid}{\mid\vec{p}\mid}$	$\leq$	$100\,\%$
	$\mid I_{R\phi} \mid$	$\leq$	$4\,cm$
	$\mid \sin\theta \times I_z \mid$	$\leq$	$8\,cm$
event cuts	E_{ch}	$\geq$	$0.15 \times \sqrt{s}$
	E_{ch}^{hem}	$\geq$	$0.03 \times \sqrt{s}$
	N_{ch}	$\geq$	7
	N_{ch}^{hem}	$\geq$	1
	$\theta_{\vec{T}}$	$\in$	$[85^\circ - 35^\circ]$

Table 1: Cuts to select hadronic events
$\vec{p}$: track momentum ; e_{neu} : neutral particle energy; t_{len} : measured track length ; $I_{R\phi(z)}$: impact parameter in $R\phi(z)$; $E_{ch}^{(hem)}$: total (hemisphere) charged energy ; $N_{ch}^{(hem)}$: total (hemisphere) multiplicity; $\sqrt{s}$: cms energy

- the TPC middle plate causes problems for the momentum measurement and charge identification.

The angular acceptance has to be reduced as well because of a decreasing b tagging capability in the forward region due to the limited coverage of the micro vertex detector.

All data collected during the years 1992 up to 1995, on and off peak, corresponding to $3.5 \cdot 10^6$ hadronic events were used in this analysis. The average centre of mass energy on peak is 91.24 GeV .

2.3 Tagging of $b\bar{b}$ events with an impact parameter method

To select a sample enriched in $b\bar{b}$ events an enhanced impact parameter method has been used. This technique is based on the well established impact parameter method which was originally proposed by ALEPH [4] and then adopted in DELPHI [5, 6]. To reach an improved capability of separating especially b from c events additional information, like the vertex mass and energy of the reconstructed secondary vertex, has been included [7].

The DELPHI Vertex Detector [3, 8], allows a very precise measurement of spatial points along the charged particles path. From 92 until 93 the vertex is fitted on an event by event basis [5], using the two dimensional information of the micro vertex detector, while the individual impact parameters are evaluated in the plane perpendicular to the colliding beams. From 94 onwards the then available z information was used in addition to calculate the vertex and the impact parameters.

For this analysis the combined probability variable, b_{tag}, has been used. $b\bar{b}$ events tend to have higher b_{tag} values whereas non-b events are peaked at smaller values (Fig.2).

Samples of events are selected by cutting on b_{tag}, where the corresponding b purities (efficiencies) increase (decrease) with higher cut values. Note that the samples selected are highly correlated because the events selected with a certain cut value are a subsample

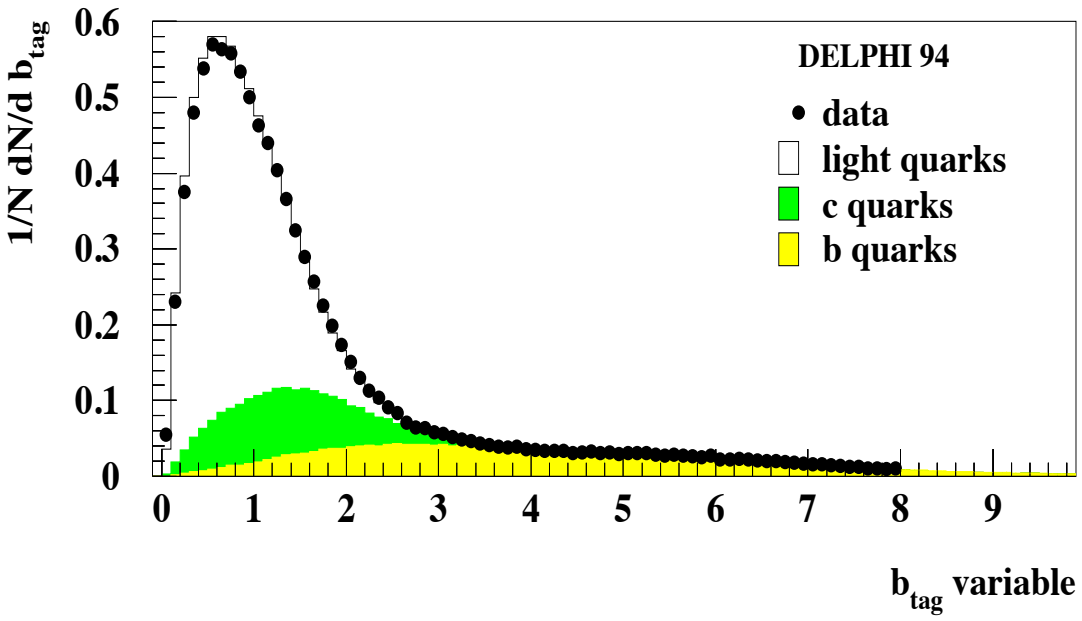

Figure 2: Comparison between Data and Monte Carlo of the normalised number of events versus the b_{tag} variable ;
light quark, c quark, and b-quark events are shown separately in the Monte Carlo case.

of the events selected for all lower cut values used.

The b purity, P_b, is defined as the fraction of $b\bar{b}$ events in the selected sample and the b efficiency, ϵ_b, is the probability of selecting a $b\bar{b}$ event, respectively. P_b is measured partly from the data using

$$P_b(cut) = \frac{\mathcal{F}(cut) - R_c \times \epsilon_c(cut) - (1 - R_c - R_b) \times \epsilon_{uds}(cut)}{\mathcal{F}(cut)} \tag{9}$$

where $\mathcal{F}$ is the fraction of selected events at a given cut value and ϵ_{uds} and ϵ_c are the selection efficiencies for the light flavours and the charm events, which are both obtained from the simulation. R_c and R_b are the fractions of $c\bar{c}$ and $b\bar{b}$ events produced in hadronic Z^0 decays and are fixed to their Standard Model values 0.172 (0.2158) for R_c (R_b). The corresponding tagging efficiencies can be estimated using Eqn.10.

$$\epsilon_b(cut) = P_b(cut) \times \frac{\mathcal{F}(cut)}{R_b} \tag{10}$$

Accurate tuning of the Monte Carlo to the data was performed [5] in order to correctly estimate the efficiencies. The data collected in different years were treated separately, due to the changes in the detector.

3 Determination of the charge separations

3.1 Charge separations of light flavours

Reliable values of the light flavour charge separations, their errors and correlations have been determined using the framework of Monte Carlo fragmentation models [9]. JETSET combined with the ARIADNE parton shower ansatz today gives the best overall description of hadronic and identified particle distributions [10, 11, 12, 13]. Therefore this model was chosen for the calculation of the quark charge separations, completed with heavy quark decays which were adjusted to recent data [15]. In the following this model will be refered as J/A fragmentation model.

The relevant calculations have been efficiently performed using an analytic substitution of the Monte Carlo model [9, 12]. The model dependence of *all charge separations* and also of *all related bins of all input distributions*, like particle rates and momentum spectra, event shapes etc. were approximated by an analytic expression $X_{MC}(p_1, ..., p_n)$ quadratic in the n model parameters p_i :

$$X_{MC}(p_1, ..., p_n) = A_0 + \sum_{i=1}^{n} B_i p_i + \sum_{i=1}^{n} C_i p_i^2 + \sum_{i=1}^{n-1} \sum_{j=i+1}^{n} D_{ij} p_i p_j \qquad (11)$$

The coefficients D_{ij} consider correlations among the model parameters. The $N = \frac{n}{2}(n + 3) + 1$ coefficients A_0, B_i, C_i and D_{ij} for each bin have been determined from a linear fit of Eqn.11 to 200 sets of Monte Carlo distributions generated with different model parameters. Each of the Monte Carlo sets has a statistic of 500.000 events. The model parameters were chosen at random in a parameter hypercube defined by the parameter intervals given in Tab.2.

The precision of this interpolation procedure has been tested by comparing the results of the analytic substitution with the real Monte Carlo answer. The average precision for all bins (including those with small statistics) was found to be 1.2% and for the charge separations (average statistical precision 0.3%) it was found to be 0.5%. No systematic bias of the predictions has been observed.

In order to determine optimal model parameters $\vec{p}_{opt}$ and the corresponding charge separations the analytic model has been fitted by minimising $\chi^2 = \sum((X_{MC} - X_{data})/\sigma_{data})^2$ [14] using different sets of data distributions (given in Tab.3). Due to imperfections of the data and the model the χ^2/N_{df} for some distributions is unacceptably large. For these distributions the errors have been rescaled according to the prescription given in [15] such that $\chi^2/N_{df} = 1$ and the fit has been repeated. The optimized parameters are given in Tab.2.

To obtain the systematic error of the charge separations δ_{f} due to uncertainties in the fragmentation model all parameters are systematically varied in the 15-dimensional hyper space. The expected Monte Carlo answer is predicted by Eqn.11 and compared to the data sets given in Tab.3. The belonging χ^2 reflects the quality of the chosen parameter setting. A cut in χ^2 is performed to discard all parameter settings leading to a χ^2 probability of less than 68%. For all parameter settings which survive the cut in χ^2 the desired charge separations δ_{f} are predicted (Eqn.11). The scattering of the charge separations reflect the uncertainty of the Monte Carlo model.

A further systematic error of this approach has been estimated by using 12 alternative combinations of input data for the determination of the central parameters. The different

No.	Parameter	Code	default	interval gen.	optimal
1	Lund a	PARJ(41)	0.5	0.3 - 1.0	0.176
2	Lund b	PARJ(42)	0.5	0.1 - 0.8	0.632
3	σ_q	PARJ(21)	0.39	0.36 - 0.42	0.357
4	Λ_{QCD}	PARA(1)	0.24	0.21 - 0.27	0.357
5	p_t^{QCD}	PARA(3)	0.7	0.3 - 0.9	0.531
6	γ_s	PARJ(2)	0.29	0.26 - 0.32	0.280
7	P(qq)/P(q)	PARJ(1)	0.1	0.085 - 0.115	0.102
8	P(us)/P(ud)/γ_s	PARJ(3)	0.5	0.3 - 0.7	1.083
9	P($ud1$)/P($ud0$)/3	PARJ(4)	0.07	0.04 - 0.10	0.046
10	Popcorn	PARJ(5)	0.5	0.06 - 4.5	0.788
11	add. baryon suppr.	PARJ(19)	0.5	0.1 - 0.9	0.397
12	P($^1S_0$)$_{ud}$	—	—	0.2 - 0.5	0.398
13	P($^3S_1$)$_{ud}$	—	—	0.2 - 0.5	0.382
14	P($^1S_0$)$_s$	—	—	0.2 - 0.5	0.483
15	P($^3S_1$)$_s$	—	—	0.2 - 0.5	0.248

Table 2: ARIADNE and JETSET parameter related to charge separations. Interval gen. denotes the interval in which the parameters of the initial Monte Carlo sets have been chosen.

combinations are presented in Tab.3. They have been selected in order to account for imperfect simultaneous description of the K^0 or $K^{\pm}$ spectra and the charged multiplicity or the x_p-distribution [12]. Furthermore event shape distributions linear or quadratic in the particle momenta have been chosen alternatively. Data set 13 will be refered as reference data set in the following, because it contains a fit to all distribution, and is mainly used for the given results.

The influence of the detector then has been considered by folding the charge flow distributions with a detector response matrix. This matrix has been determined using the full simulation of the DELPHI apparatus. For a generated charge flow in a given bin it determines the probability to measure the charge flow in any other bin of the distribution. As this matrix can only be determined for events which have been accepted in the analysis a further correction factor has been applied to account for a possible bias due to the events rejected by the measuring process or cuts applied in the analysis.

The mean values of the charge separations $\delta_{\mathrm{u,d,s,c}}$ using the reference data set are given in Tab.4 for the detector setting of 94. Because the charge separations have to be folded with the response of the DELPHI detector they cannot be directly compared to the corresponding results of other experiments. Only the ratios of the different flavours should be compatible. Comparing the different years of data taking the values change slightly, which is due to a different acceptance of tracks and events depending on the different flavours.

distribution	data set												
	1	2	3	4	5	6	7	8	9	10	11	12	13
x_p [D] ρ^0 [A,D] ω [A] f^0, f^2 [D] K^{*0} [A,D,O] $K^{*\pm}$ [A,D,O] Proton [A,D] Ξ, Ξ^* [A] $y(p) - y(\bar{p})$ [A] $y(\Lambda) - y(\bar{\Lambda})$ [O] Δ^{++} [D,O] Λ^0 [A,D] Σ_{1385} [D,O]	•	•	•	•	•	•	•	•	•	•	•	•	•
charged multiplicity							•	•	•	•	•	•	•
Thrust, Major, Minor [D] $p_t^{in/out}$ (Thrust) [D] Rapidity (Thrust) [D] $D_{2,3}$ Durham [D]	•		•		•		•		•		•		•
Spher., Aplan., Plan. [D] $p_t^{in/out}$ (Spher.) [D] Rapidity (Spher.) [D] $D_{2,3}$ Jade [D]		•		•		•		•		•		•	•
K^0 [A]	•	•			•	•	•	•			•	•	•
$K^{\pm}$ [A]			•	•	•	•			•	•	•	•	•

Table 3: Combinations of input data used for the determination of the charge separations (data set 13) and for the systematic cross check (data set 1-12). The • denotes the data belonging to the dataset. [A] means ALEPH Measurement, [D] DELPHI means Measurement and [O] means OPAL Measurement.

κ	$\delta_{\rm d}$	$\delta_{\rm u}$	$\delta_{\rm s}$	$\delta_{\rm c}$
0.3	-0.1406	0.2392	-0.1816	0.1677
0.5	-0.1638	0.2870	-0.2308	0.1735
0.8	-0.1963	0.3540	-0.3005	0.1746
1.0	-0.2151	0.3917	-0.3408	0.1734
1.2	-0.2299	0.4229	-0.3753	0.1717
2.1	-0.2708	0.4075	-0.4692	0.1615

Table 4: Charge separations as determined with the J/A model and folded with the DELPHI detector of 94.

The influence of the b tagging leads to a bias of the charge separations. A correction has been determined from the DELPHI simulation and accounts for differences in the b purity dependence. At the working point of $P_{\rm b} = 92\%$ and $\epsilon_{\rm b} = 75\%$ the correction which have to be applied are given in Tab.5 for different quark flavours.

κ	$\mathcal{C}_{\rm d}$	$\mathcal{C}_{\rm u}$	$\mathcal{C}_{\rm s}$	$\mathcal{C}_{\rm c}$
0.3	0.65 ± 0.051	0.80 ± 0.038	0.72 ± 0.046	0.86 ± 0.015
0.5	0.67 ± 0.050	0.82 ± 0.036	0.74 ± 0.041	0.81 ± 0.016
0.8	0.69 ± 0.053	0.84 ± 0.038	0.76 ± 0.040	0.71 ± 0.021
1.0	0.70 ± 0.057	0.86 ± 0.040	0.76 ± 0.041	0.65 ± 0.025
1.2	0.72 ± 0.060	0.87 ± 0.042	0.76 ± 0.042	0.58 ± 0.030
2.1	0.75 ± 0.074	0.91 ± 0.049	0.76 ± 0.048	0.37 ± 0.046

Table 5: Correction factors with their statistical error on $\delta_{\rm d,u,s,c}$ for different κ's at the working point for 1994 data ($\mathcal{C}_{\rm f} = \delta_{\rm f}(P_{\rm b})/\delta_{\rm f}$; $P_{\rm b} = 92\%$)

To account for the angular dependence of the differential asymmetry, the $A_{FB}^{\rm b\bar{b}}$ measurement is performed in 4 different bins of $\theta_{\vec{T}}$. The light quark charge separations are extracted using the complete selected region. Correction factors to account for the different $\theta_{\vec{T}}$ bins are taken from the simulation and are listed in Tab.6 for the chosen working point.

$\theta_{\vec{T}}$	$\mathcal{C}_{\rm d}$	$\mathcal{C}_{\rm u}$	$\mathcal{C}_{\rm s}$	$\mathcal{C}_{\rm c}$
$75^\circ - 85^\circ$	1.03 ± 0.17	0.94 ± 0.10	1.06 ± 0.12	0.91 ± 0.06
$65^\circ - 75^\circ$	0.88 ± 0.16	1.00 ± 0.10	1.02 ± 0.12	1.01 ± 0.06
$50^\circ - 65^\circ$	0.91 ± 0.15	0.96 ± 0.09	0.95 ± 0.10	1.04 ± 0.06
$35^\circ - 50^\circ$	1.26 ± 0.20	1.17 ± 0.12	0.98 ± 0.14	1.03 ± 0.08

Table 6: Correction factors with their statistical error on $\delta_{\rm d,u,s,c}$ for different $\theta_{\vec{T}}$ bins for 1994 data ($\mathcal{C}_{\rm f} = \delta_{\rm f}(\theta_{\vec{T}})/\delta_{\rm f}$; $\kappa = 0.8$)

This corrections are small, stable over the $P_{\rm b}$ range and show little dependence on κ

and on the year of data taking.

3.2 b charge separation

The b charge separation can be measured on data from the widths of the charge flow and the total charge distributions with very small input from the simulation. This has the advantage of being independent of the Monte Carlo description of the poorly known B hadron decays. A discrepancy between the extracted $\delta_{\rm b}$ and the value inside the simulation is therefore expected.

A single measurement of the hemisphere charge can be regarded as sum of three independent terms:

$$Q_{\rm f} = \frac{\delta_{\rm f}}{2} + \frac{E_{\rm f}}{2} + S_{\rm f} \qquad Q_{\bar{\rm f}} = \frac{-\delta_{\rm f}}{2} + \frac{E_{\bar{\rm f}}}{2} + S_{\bar{\rm f}} \tag{12}$$

where $E_{\rm f}$ ($=E_{\bar{\rm f}}$) is a non vanishing (positive) bias due to hadronic re-interactions in the detector material and $S_{\rm f(\bar{f})}$ accounts for statistical variations of $Q_{\rm f(\bar{f})}$, thus $\langle S_{\rm f(\bar{f})} \rangle = 0$.

From the two equations above one can obtain:

$$\sum_{\rm f=u,d,s,c,b} P_{\rm f}\delta_{\rm f}^2 = \sigma_{FB}^2 - \sigma_{TOT}^2 + \langle Q_{FB} \rangle^2 + \underbrace{\sum_{\rm f=u,d,s,c,b} P_{\rm f}(4\langle S_{\rm f} S_{\bar{\rm f}} \rangle + E_{\rm f}^2) - (\sum_{\rm f=u,d,s,c,b} P_{\rm f} E_{\rm f})^2}_{\rm MC} \tag{13}$$

This equation describes the relation between $\delta_{\rm b}$ and the other measurable quantities. Most of the right hand side of this equation can be extracted from data, apart from the last terms, marked with the under brace. They are numerically small and can be safely estimated from simulation. It should be noted that the $E_{\rm f}$ term cancels completely in Eqn.13 if $P_{\rm b} = 1$ or if $E_{\rm f}$ is flavour independent. Left over are the $\langle S_{\rm f} S_{\bar{\rm f}} \rangle$ terms accounting for the small hemisphere-hemisphere charge correlation, which is due to charge conservation, due to the common Thrust axis and due to occasional particle crossovers between hemispheres.

The right hand side of Eqn.13 is evaluated in samples of increasing b purity, which were obtained by selecting events lying above a certain $\rm b_{tag}$ value. The b charge separation can be extracted directly when subtracting the background part $\sum_{\rm f \neq b} P_{\rm f}\delta_{\rm f}^2$ and separating $\delta_{\rm b}$.

The measured $\delta_{\rm b}$ is shown over the complete b purity range in Fig.3 for two different κ values in the lower plot. In the high purity region the resulting $\delta_{\rm b}$ is nearly stable. The remaining slope is well reproduced in the simulation and due to a small bias because of the b tagging applied. In the region below 70% the slope is more pronounced and not well reproduced in the simulation. In this intermediate or low b purity region $\epsilon_{\rm u,d,s}$ but rather $\epsilon_{\rm c}$ is not well understood, which leads to problems in the method of the $P_{\rm b}$ and $\epsilon_{\rm b}$ calculation. This is of no importance, as only the values at high $P_{\rm b}$ enter into the analysis.

The measured mean squared charge separation (upper plot) and the term deduced from the Monte Carlo , which includes the hemisphere correlation term, (middle plot) are shown in addition. Note that the points are highly correlated. This extraction procedure has been checked on simulated data where it reproduced the input charge separation correctly.

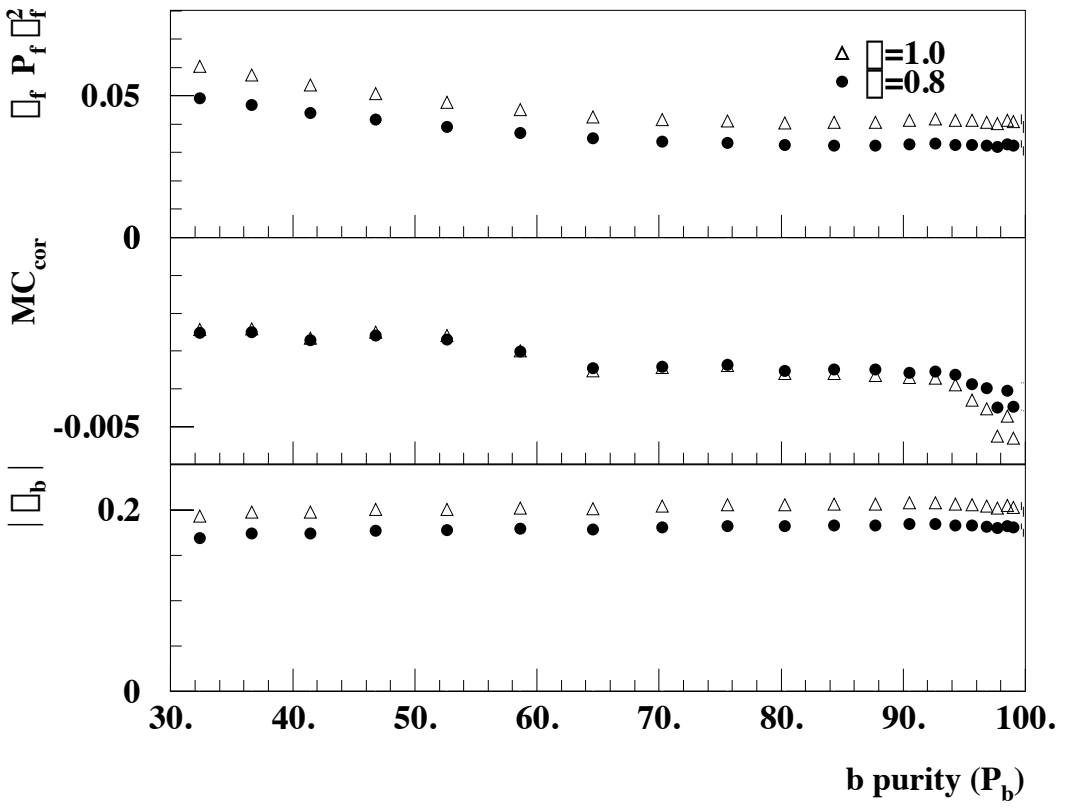

Figure 3: Measurement of $\delta_{\rm b}$ for different κ values upper plot : $\sum_{\rm f} P_{\rm f}\delta_{\rm f}^2$, middle plot : Monte Carlo correction $\mathrm{MC_{cor}}$, lower plot : calculated $\delta_{\rm b}$

year	$\delta_{\rm b}(\kappa = 0.3)$	$\delta_{\rm b}(\kappa = 0.5)$	$\delta_{\rm b}(\kappa = 0.8)$
92	$-0.1184 \pm 0.00260(14)$	$-0.1470 \pm 0.00290(14)$	$-0.1871 \pm 0.00390(16)$
93	$-0.1191 \pm 0.00310(16)$	$-0.1463 \pm 0.00350(16)$	$-0.1850 \pm 0.00480(16)$
94	$-0.1166 \pm 0.00170(15)$	$-0.1446 \pm 0.00190(11)$	$-0.1843 \pm 0.00260(15)$
95	$-0.1176 \pm 0.00300(15)$	$-0.1452 \pm 0.00330(12)$	$-0.1838 \pm 0.00460(16)$
year	$\delta_{\rm b}(\kappa = 1.0)$	$\delta_{\rm b}(\kappa = 1.2)$	$\delta_{\rm b}(\kappa = 2.1)$
92	$-0.2114 \pm 0.00480(15)$	$-0.2331 \pm 0.00570(16)$	$-0.2992 \pm 0.00920(20)$
93	$-0.2079 \pm 0.00580(12)$	$-0.2282 \pm 0.00700(14)$	$-0.2882 \pm 0.01140(15)$
94	$-0.2081 \pm 0.00320(12)$	$-0.2289 \pm 0.00390(15)$	$-0.2882 \pm 0.00640(18)$
95	$-0.2069 \pm 0.00560(10)$	$-0.2273 \pm 0.00670(11)$	$-0.2854 \pm 0.01110(14)$

Table 7: Calculated $\delta_{\rm b}$ values at the working point for the 4 years of data taking

The extracted $\delta_{\rm b}$ values used for the analysis at a working point of $P_{\rm b} = 92\%$ are given in Tab.7 for the different years. The error of the charge separation given in parenthesis is due to the systematics of the determination of the light and charm charge separation.

Similar to the light and charm charge separation case correction factors which account for the different $\theta_{\vec{T}}$ bins are taken from the simulation (Tab.8). The variation of the correction factors with increasing $P_{\rm b}$ and the dependence on κ is very small. Within their statistical errors they are equal for the different years of data taking.

$\theta_{\vec{T}}$	$\mathcal{C}(\kappa = 0.3)$	$\mathcal{C}(\kappa = 0.5)$	$\mathcal{C}(\kappa = 0.8)$
$75^\circ - 85^\circ$	0.963 ± 0.0096	0.965 ± 0.0090	0.967 ± 0.0092
$65^\circ - 75^\circ$	1.008 ± 0.0093	1.006 ± 0.0087	1.005 ± 0.0089
$50^\circ - 65^\circ$	1.024 ± 0.0080	1.024 ± 0.0075	1.024 ± 0.0077
$35^\circ - 50^\circ$	0.993 ± 0.0099	0.992 ± 0.0091	0.991 ± 0.0092
$\theta_{\vec{T}}$	$\mathcal{C}(\kappa = 1.0)$	$\mathcal{C}(\kappa = 1.2)$	$\mathcal{C}(\kappa = 2.1)$
$75^\circ - 85^\circ$	0.968 ± 0.0095	0.968 ± 0.0099	0.969 ± 0.0111
$65^\circ - 75^\circ$	1.005 ± 0.0092	1.006 ± 0.0096	1.006 ± 0.0108
$50^\circ - 65^\circ$	1.024 ± 0.0080	1.023 ± 0.0083	1.022 ± 0.0093
$35^\circ - 50^\circ$	0.991 ± 0.0095	0.991 ± 0.0098	0.991 ± 0.0110

Table 8: Correction factors with their statistical error on $\delta_{\rm b}$ for different $\theta_{\vec{T}}$ bins for 1994 data

For completeness $\langle Q_{TOT} \rangle$,the H term(Eqn.14) and $\sigma^2_{FB} - \sigma^2_{TOT}$ are shown as well, because they enter in the determination of $\delta_{\rm b}$ (Fig.4). $\langle Q_{TOT} \rangle = \sum_{\rm f=u,d,s,c,b} P_{\rm f} E_{\rm f}$ has been taken from the simulation because of the cancelling effect mentioned. The discrepancies in the $\langle Q_{TOT} \rangle$ measurement are due to an inaccurate description of the secondary interactions in the simulation and enter in most of the hemisphere charge related observables. This disagreement is less important because the value enters only via the numerically small Monte Carlo correction term. The H term, where this differences are mostly reduced by the subtraction of the $\langle Q_{TOT} \rangle$ term, enters not directly. It is close to the hemisphere-hemisphere correlation and strongly related to $\langle Q_F Q_B \rangle$, and has been taken as well from the simulation:

$$\mathrm{H} = \langle Q_F Q_B \rangle - \langle Q_{TOT} \rangle^2 / 4 \tag{14}$$

A sufficient agreement between data and simulation has been found and ensures the validity of the $\delta_{\rm b}$ determination. $\sigma^2_{FB} - \sigma^2_{TOT}$ has been taken from the data and the deviation between data and simulation reflect that the $\delta_{\rm b}$ value inside the simulation is different from the measured one.

4 The measurement of $A^{\rm b\bar{b}}_{FB}$

The major input variable for the measurement of $A^{\rm b\bar{b}}_{FB}$ is $\langle Q_{FB} \rangle$. For the evaluation of $A^{\rm b\bar{b}}_{FB}$ Eqn.6 has been used. $\langle Q_{FB} \rangle$ is shown in comparison with the simulation in Fig.5 for the complete selected angular region.

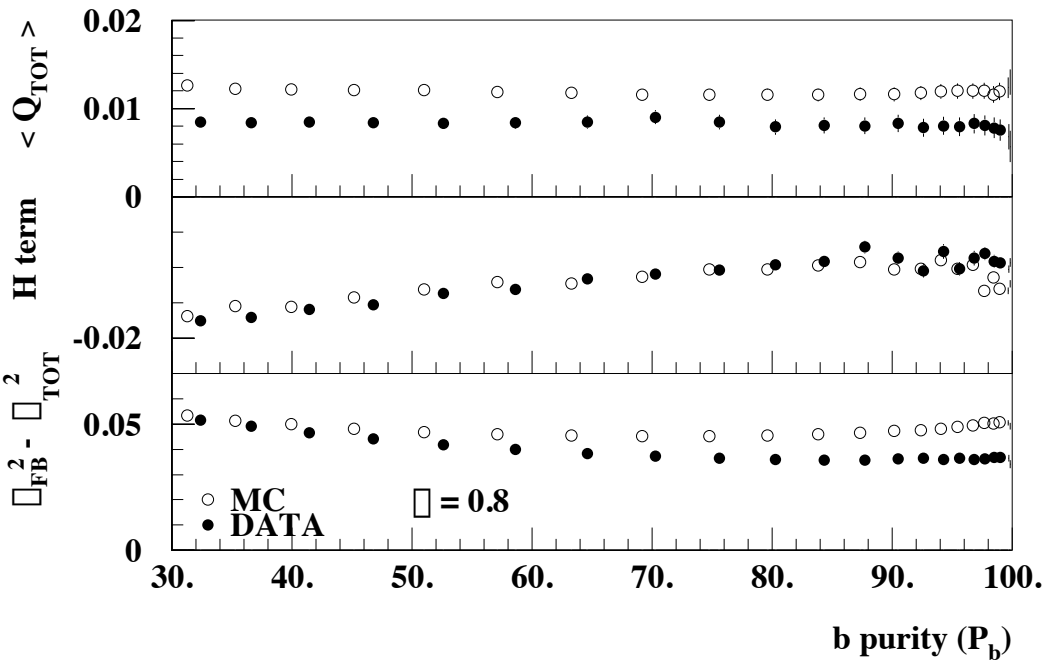

Figure 4: $\langle Q_{TOT} \rangle$, H term and $\sigma^2_{FB} - \sigma^2_{TOT}$ variable, in comparison data and simulation for $\kappa = 0.8$ for 1994 data.

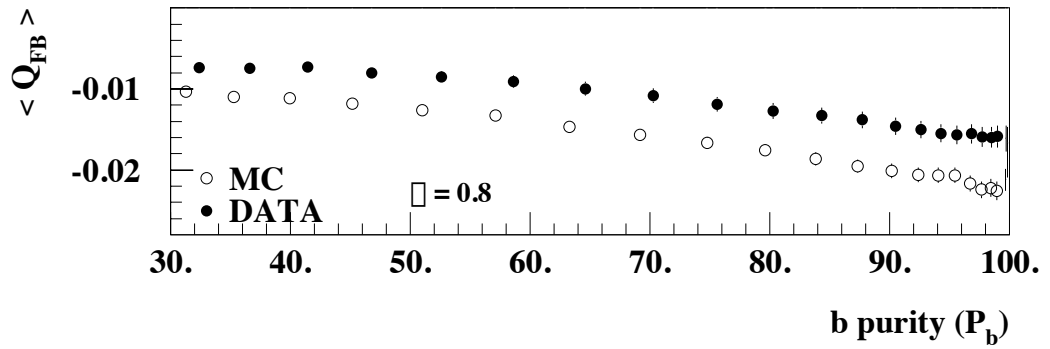

Figure 5: $\langle Q_{FB} \rangle$ as obtained from data and simulation for $\kappa = 0.8$ for 1994 data.

For the $A_{FB}^{\mathrm{b\bar{b}}}$ evaluation $\langle Q_{FB} \rangle$ has been calculated for the 4 $\theta_{\vec{T}}$-bins separately: $35^\circ - 50^\circ$, $50^\circ - 65^\circ$, $65^\circ - 75^\circ$ and $75^\circ - 85^\circ$. The discrepancy between data and simulation is similar for all bins. The determination of the other quantities entering in Eqn.6 and Eqn.9 is discussed below with the exception of the charge separations which have been discussed already.

4.1 The tagging purities P_{f} and efficiencies ϵ_{f}

The effects of different acceptance for the quark flavours has been estimated from the simulation. The usage of the b tagging requires systematical studies of the purities P_{f} and efficiencies ϵ_{f}.

The b fraction, P_{b}, and efficiency, ϵ_{b}, are measured directly from the data using R_{b} and R_{c} from the standard model prediction (see Eqn. 9,10). The purities and efficiencies for light and charm quarks are taken from the simulated data sample. The contribution of charm events has to be checked in detail because charm events have an opposite asymmetry compared with the down-type quark b. Long lived charm fragmentation products may be found even after applying a high cut on the b tagging probability. At large b tagging probability ($P_{\mathrm{b}} = 92\%$) about 75% of the remaining background is due to charm events. For example the lifetimes and fractions of D-meson in c events have been checked carefully.

4.2 The angular correction factor η_{f}

The angular acceptance of the analysis is limited below 35° in polar angle due to detector acceptance and decreasing momentum resolution of the tracking system at small angles. The part around 90° has been rejected because the measurement of δ_{b} is distorted due to detector effects and in addition does not contribute to the asymmetry measurement. As the differential asymmetry increases with the polar angle a correction factor η has to be applied. Neglecting mass and QCD effects from the shape of the differential cross section this correction factor can be written as:

$$\eta_1^{\mathrm{f}} \;=\; \frac{8}{3} \frac{\int_0^1 \epsilon_{\mathrm{f}}(\cos\theta) \cos\theta \; d\cos\theta}{\int_0^1 \epsilon_{\mathrm{f}}(\cos\theta)(1 + a\cos^2\theta) \; d\cos\theta} \tag{15}$$

$\epsilon_{\mathrm{f}}(\cos\theta)$ is the flavour dependent selection efficiency. When considering the Thrust axis ($\vec{T}$) as the reference direction, $a = 0.95$, while taking the quark axis ($\vec{\mathrm{q}}$) before gluon radiation into account (which then accounts in addition for effects introduced by the selection) $a = 1$ (see [16]).

The radiation of hard gluons for events at initially very small polar angles θ and losses of particles in the dead areas of the detector close to the beam may cause these events to be accepted in the analysis. A correction for this effect which depends on the amount of gluon radiation can be calculated using:

$$\eta_2^{\mathrm{f}} \;=\; \frac{Q_{FB}^{\mathrm{f}}}{\delta_{\mathrm{f}} A_{FB}^{\mathrm{f},gen}} \tag{16}$$

In order to reduce the statistical error of this correction η_2^{f} has been calculated with an artificially enlarged generated asymmetry of 0.75 assuming a perfectly forward/backward

flavour	$\eta_1(\vec{q})$	$\eta_2(\kappa = 0.8)$
d	0.922 ± 0.028	0.950 ± 0.08
u	0.920 ± 0.032	0.956 ± 0.06
s	0.921 ± 0.028	0.912 ± 0.06
c	0.894 ± 0.009	0.943 ± 0.03
b	0.935 ± 0.001	0.930 ± 0.005

Table 9: Comparison between the different definitions of the angular correction for 1994 data

symmetric detector. A breakdown of the different correction factors η for 1994 data is given in Tab.9 in order to depict the magnitude of the different corrections .

For the determination of the central values always η_2 is used, as it includes the effects of the limited angular acceptance, smearing and QCD effects. The QCD correction term can be calculated by $\eta_2/\eta_1(\vec{q})$ and is compatible with 1. This was expected, because the method of extracting the charge separations should include all QCD dependent terms.

The rather big errors for the light and c quarks are due to the small statistic in this high purity region and habe little influence on the result. η_1 is per construction κ independent, while η_2 shows no κ dependence within the error. Both quantities vary with increasing P_{b} and the values change slightly for the different years.

4.3 The determination of $A_{FB}^{\mathrm{b\bar{b}}}$

The angular correction factor η has been calculated separately for the $\theta_{\vec{T}}$ bins using Eqn.16. The purities have been computed as well for each angular bin, whereas δ_{b} has been measured on the bases of the full selected angular region and corrected afterwards using the simulation. The light and charm quark charge separations have been evaluated using the Monte Carlo fragmentation model. The resulting values have been corrected using the simulation for detector effects, for the b purity dependence and analogous to δ_{b} for the angular bining. No additional b mixing correction has been applied, because this is already included in the δ_{b} measurement.

It has been checked that the $A_{FB}^{\mathrm{b\bar{b}}}$ extracted for the different $\theta_{\vec{T}}$ bins are compatible among themselves and with the average asymmetry. The relation between $A_{FB}^{\mathrm{b\bar{b}}}$ and $A_{FB}^{\mathrm{c\bar{c}}}$ has been taken from the SM and an up/down type universality has been assumed ($A_{FB}^{\mathrm{b\bar{b}}}$ $=A_{FB}^{\mathrm{s\bar{s}}}$ $=A_{FB}^{\mathrm{d\bar{d}}}$, $A_{FB}^{\mathrm{c\bar{c}}}$ $=A_{FB}^{\mathrm{u\bar{u}}}$). The determination has been performed for 6 κ values and for the full range of P_{b}. The results are highly correlated in both cases.

The working point has been chosen to minimize the expected total error on $A_{FB}^{\mathrm{b\bar{b}}}$ from the simulation to $\kappa = 0.8$. For all years this turns out to be the region of about 92% b purity. The results are given for different κ's at the working point in Fig.6. Only the statistical errors are shown.

The κ dependence is slightly different between the years, which is due to a different detector response. Within one year the values for different κ's are compatible.

For three different κ's (0.5,0.8,1.0) the variation with P_{b} is given individually for all the years in Fig.7. Note again that the data points are highly correlated. The working point is marked by the arrow in the middle plot.

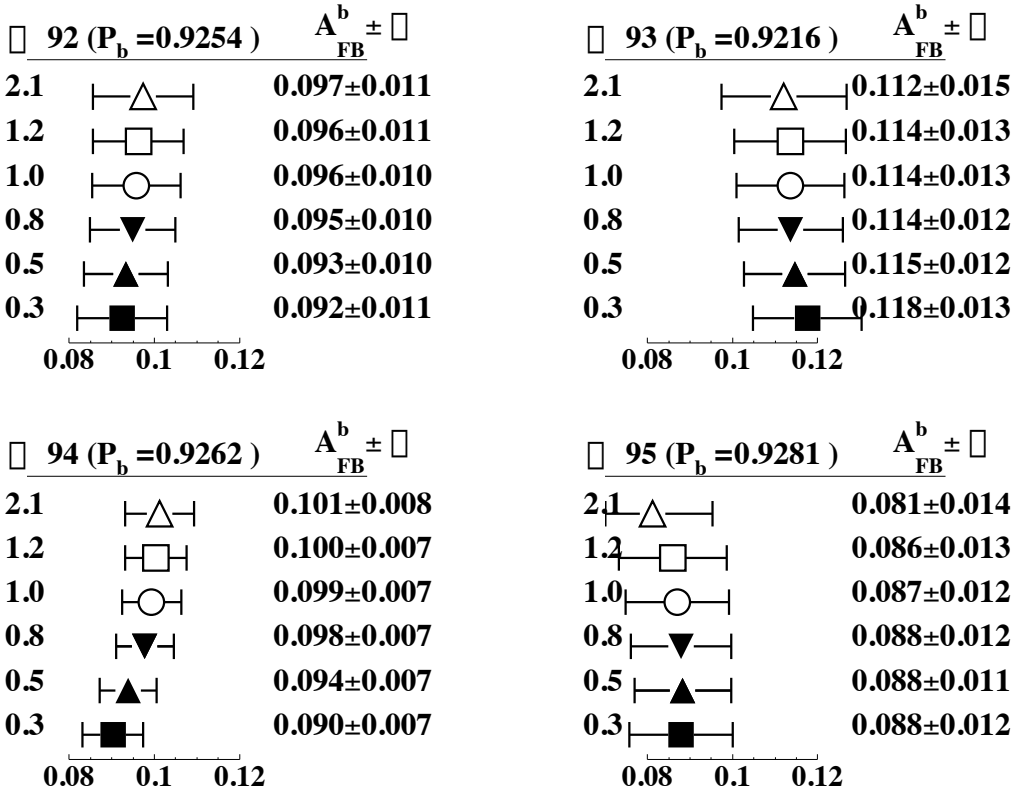

Figure 6: Results of the $A_{FB}^{b\bar{b}}$ measurement with statistical error depending on κ. For all years only the selected working point is shown.

The extracted $A_{FB}^{b\bar{b}}$ values are stable above $P_b \sim 80\%$ while in the low purity region some problems in describing the background are visible (see section 3.2). The results of the individual years are compatible within the stable region.

5 Systematic error

Systematic uncertainties introduced by the b tagging

In order to determine the systematic uncertainties of P_b and ϵ_b the quantities entering in Eqn.9 were individually studied and varied.

R_c (R_b) was set to the Standard Model values 0.172 (0.2158) and changed by $\pm 5\%$ ($\pm 0.5\%$) for systematic studies. The dependence between the measured values and R_c, respectively R_b, can be approximated by a linear dependence. The chosen variation results in systematic uncertainties, which are given in Tab.11.

The efficiencies for light and charm quarks enter also and a careful study was done as proposed in [17]. Both ϵ_{uds} and ϵ_c depend on the detector performance and were treated for each year separately, as well as the tuning of the b tagging. Different influences on

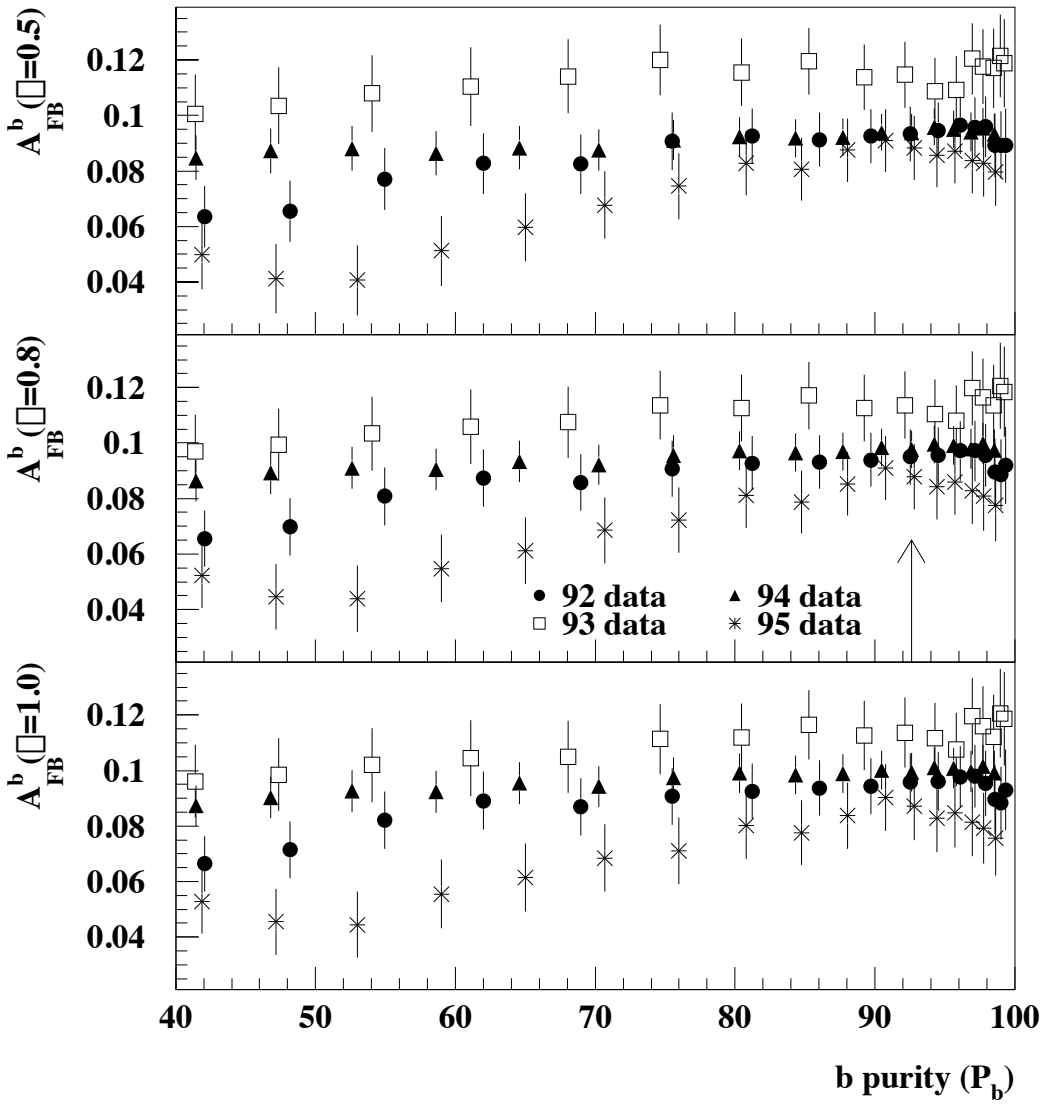

Figure 7: Results of the $A_{FB}^{\mathrm{b\bar{b}}}$ measurement with statistical errors depending on P_{b} for $\kappa = 0.5, 0.8, 1.0$ for all the years.

$\epsilon_{\rm uds}$ were studied:

- The gluon splitting into $c\bar{c}$ or $b\bar{b}$ pairs inside light quark events. A conservative change of $\pm 50\%$ for each channel was taken into account. These splittings lead to lifetime information and enter into the b purity measurement.

- The K^0 and Λ content in light quark events was varied by $\pm 10\%$ as these contributions may bias the b tagging.

- To estimate the effect of the detector resolution the probability depending only on the impact parameter information has been used. $F_E^+(F_E^-)$ is the event probability for positive(negative) measured impact parameters. The difference between the number of events fulfilling the same F_E^- cut in data and Monte Carlo gives an estimate of the resolution contributing to $\epsilon_{\rm uds}$ in the associated F_E^+ bin. These bins have been related to the $b_{\rm tag}$ bining and the corresponding $P_{\rm b}$.

The tagging efficiency $\epsilon_{\rm c}$ inside the b enriched sample is more critical than the contributions mentioned before.

- The fractions of D meson production in c events was systematically studied according to the procedure proposed in [17]. The uncertainties were estimated by varying the corrected values inside the uncertainties given in Tab.10. Each systematic shift of the D^+,D_s,Λ_c contribution was compensated by the D^0 fraction, therefore no extra error is given in that case.

- Shifts induced to $P_{\rm b}$, $\epsilon_{\rm b}$ and arising from the uncertainties of the D lifetimes were estimated by varying the corrected lifetimes within the errors quoted in Tab.10. The correction factor uses the exponential dependence of the lifetimes.

- The influence of the uncertainty of the average scaled momentum $\langle X_E \rangle$ of the D's was studies by re-weighting the events such that the resulting $\langle X_E \rangle$ changes by $\pm 2\%$ corresponding to the uncertainty of the measurement 0.480 ± 0.008 [17]. The measurement was corrected for gluon splitting, nevertheless for systematic studies the 2 or 6 fastest mesons were taken into account and the resulting variation on the asymmetry turns out to be equal within errors.

- The events were re-weighted according to the K^0 decay rate and depending on the primary D meson inside the c events [15].

- The charged multiplicity in charm events was varied according to the inclusive topological branching ratios measured for D^0,D^+ and D_s [18].

Systematic uncertainties introduced by the η-factor and the QCD correction

As mentioned in section 4.2 two different definitions of $\eta^{\rm f}$ are reasonable. For the determination of $A_{FB}^{b\bar{b}}$ the definition $\eta_2^{\rm f}$ has been always used. But for an estimate of the systematic uncertainty coming from the selection and the cut into the acceptance region $\eta_1^{\rm f}$ has been considered in addition. The advantage of this definition is that $\eta_1^{\rm b}$ can be calculated on data and on Monte Carlo. A maximum difference of 0.5 % at $P_{\rm b} = 92\%$

D-Meson	fraction	lifetime $[ps]$
D^0	0.600	0.415 ± 0.004
D^+	0.233 ± 0.028	1.057 ± 0.015
D_s	0.102 ± 0.037	0.467 ± 0.017
Λ_c	0.065 ± 0.029	0.206 ± 0.012

Table 10: Measurement of D meson fraction inside c quarks and of their lifetimes

has been found considering all years. For the light and c quarks a conservative systematic error of 5% has been taken into account, which is the maximum difference between $\eta_1^{\mathrm{f}\neq\mathrm{b}}$ and $\eta_2^{\mathrm{f}\neq\mathrm{b}}$, where both numbers have been calculated on Monte Carlo.

Systematics coming from the Thrust axis resolution were studied and found to be negligible. The experimental thrust axis resolution, when applying the angular acceptance cut, caused an excess of small angle events to enter the acceptance region. The related bias on $A_{FB}^{\mathrm{b\overline{b}}}$ was estimated with simulation.

Systematic uncertainties introduced by the udsc charge separations

As mentioned in section 3.1 the uncertainty due to the charge separations was divided into three different sources. The precision of the interpolation procedure, the uncertainty due to the Monte Carlo parameters (see section 3.1) and at least the uncertainty due to the choice of the input distributions. The first source gives negligible effects on the result. The second was treated by repeating the $A_{FB}^{\mathrm{b\overline{b}}}$ extraction with Eqn.6 50 times. The third was studied by solving this equation with 13 different charge separation data tuned separately by using different input distributions. It turns out that the influence of the different data sets is very small. Using 50 different charge separation sets of the reference data set 13 results as well to a small systematic error on the asymmetry.

An additional uncertainty arises from the acceptance correction procedure, which is performed in two steps. In the first step the generated $Q_{FB}^{\mathrm{f},F}$ distribution is folded with a correction matrix obtained from a detailed simulation of the DELPHI detector. Their elements are the probability ε_{ij} to measure an event inside bin i, instead of bin j, where it was generated. Therefore the content inside the bin i can be expressed by:

$$N_i' = \sum_{j=1}^{N} \varepsilon_{ij} N_j \tag{17}$$

where N is the number of bins. The accepted charge separation is given by the mean of the projected distribution:

$$\delta_{\mathrm{f}}^{acc} \quad = \quad \frac{1}{N} \sum_{i=1}^{N} N_i' Q_{FB}^{\mathrm{f},F,i} \tag{18}$$

The elements of this correction matrix can only be computed in the case, where the event has passed the event selection. To avoid any bias an extra factor has been applied. Half of the deviation of this correction from unity was considered as systematic error.

Contribution	$\Delta A_{FB}^{\mathrm{b\bar{b}}} \times 10^2$
Charge separation δ_{udsc}	0.013
Angular correction	0.050
R_{b} + 0.5%	0.001
R_{c} - 5%	0.040
H charge correlation	0.110
hadronic interaction	0.027
Detector resolution (light,charm)	0.130
Gluon splitting $g \to \mathrm{c\bar{c}}$, $g \to \mathrm{bb}$	0.016
Charm systematics	0.089

Table 11: Systematic uncertainties and their influence on the $A_{FB}^{\mathrm{b\bar{b}}}$ determination

Systematic uncertainties due to detector effects

The stability of the results due to the variations of the selection cuts was studied and the corresponding systematic error was evaluated.

The hemisphere-hemisphere correlation term $\langle S_{\mathrm{f}} S_{\bar{\mathrm{f}}} \rangle$ is mainly given by the introduced H term for which a discrepancy of about 20% between data and Monte Carlo has been found (depending on the year). As systematic uncertainty for this correlation term the same order of magnitude has been assumed.

To account for inaccurate description of the hadronic interaction, the tracks have been reweighted in such a way, that $\langle Q_{TOT} \rangle$ in the simulation becomes equal to the corresponding data value. The full analysis has been performed and the difference in the $A_{FB}^{\mathrm{b\bar{b}}}$ measurement has been taken as systematic uncertainty.

All the systematic error contributions are summarised in Tab.11.

6 Conclusions

A measurement of $A_{FB}^{b\bar{b}}$ using an impact parameter tag and a jet charge technique has been performed. The analysis includes all data collected with the DELPHI detector from 1992 to 1995. The asymmetries for the individual years of data taking are:

$$\begin{array}{lrcl} 92\ (91.28\ \text{GeV}): & A_{FB}^{b\bar{b}} & = & 0.0950 \pm 0.0101(\text{stat.}) \\ 93\ (91.22\ \text{GeV}): & A_{FB}^{b\bar{b}} & = & 0.1137 \pm 0.0122(\text{stat.}) \\ 94\ (91.20\ \text{GeV}): & A_{FB}^{b\bar{b}} & = & 0.0977 \pm 0.0068(\text{stat.}) \\ 95\ (91.29\ \text{GeV}): & A_{FB}^{b\bar{b}} & = & 0.0879 \pm 0.0118(\text{stat.}) \end{array}$$

Combining these independent measurements at a centre of mass energy of 91.26 GeV yields:

$$A_{FB}^{b\bar{b}} \quad = \quad 0.0979 \pm 0.0047(\text{stat.}) \pm 0.0021(\text{syst.})$$

From which a value of $\sin^2\theta^{l}_{\text{eff}}$ is obtained:

$$\sin^2\theta^{l}_{\text{eff}} \quad = \quad 0.2320 \pm 0.0009$$

Both results are in good agreement with the SM and compatible to the recent published data of other experiments.

Acknowledgements

We are greatly indebted to our technical collaborators and to the funding agencies for their support in building and operating the DELPHI detector, and to the members of the CERN-SL Division for the excellent performance of the LEP collider.

References

[1] The LEP Collaborations, Phys. Lett. B276 (1992) 267.

[2] DELPHI Collaboration, P.Abreu et al., Nucl.Instr.Meth. **A303** (1991) 233.
DELPHI Collaboration, P.Abreu et al., Nucl.Instr.Meth. **A378** (1996) 57.

[3] N. Bingefors et al. Nucl.Instr.Meth. **A328** (1993) 447.

[4] ALEPH Collaboration, D.Buskulic et al., Phys.Lett. **B313** (1993) 535.

[5] G.V.Borisov, Lifetime tag of events $Z^0 \to b\bar{b}$ with the DELPHI detector. AABTAG program. , DELPHI note 94-125;
G.V.Borisov and C.Mariotti, Final tuning of track impact parameter resolution of the DELPHI Detector, DELPHI 95-142 PHYS 567.

[6] DELPHI Collaboration, P.Abreu et al., Z. Phys. **C65** (1995) 555.

[7] DELPHI Collaboration, G.J. Barker et al., *A precise measurement of the partial decay width ratio* $R_b^0 = \Gamma_{b\bar{b}}/\Gamma_{had}$ *at the* Z, ICHEP'98 #123, Vancouver, DELPHI 98-123 CONF 184.

[8] The Silicon Tracker in the DELPHI Experiment at LEP2, DELPHI 97-121 Conf 103, HEP'97, Jerusalem.

[9] U. Flagmeyer, Diplomarbeit, WUD 96-25, Bergische Univ.-GH, Wuppertal (1996).

[10] T. Sjöstrand, Comp. Phys. Comm. 39 (1986) 347; T. Sjöstrand and M. Bengtsson, Comp. Phys. Comm. 46 (1987) 367.

[11] L. Lönnblad, Comp. Phys. Comm. 71 (1992) 15.

[12] DELPHI Collab., P. Abreu et al.,Z. Phys. C73 (1996) 11-59.

[13] W. Neumann, Dissertation, WUB-DIS 97-11, Bergische Univ.-GH, Wuppertal (1997).

[14] F. James and M. Goossens, *Minuit, Function Minimization and Error Analysis*, Reference Manual, CERN Program Library Long Writeup, D506 (1992).

[15] The Particle Data Group, R.M. Barnett et al., Phys. Rev. D54, 1, (1996).

[16] The LEP Electroweak Working Group, Presentation of LEP Electroweak Heavy Flavour Results for Summer 1996 Conferences, LEPHF/96-01

[17] The LEP Electroweak Working Group, ALEPH Note 94-30, DELPHI 94-23 Phys 357, L3 Note 1577, OPAL Technical Note TN213, 28 February, 1994;
The LEP Electroweak Working Group, ALEPH Note 94-90, DELPHI 94-23 Phys 357/add, L3 Note 1613, OPAL Technical Note TN237, 10 June, 1994.

[18] MARK III Coll., D. Coffman et al., Phys. Lett. B263 (1991) 135.